TU Delft

Delft University of Technology

Document Version
Final published version

Licence
CC BY

Citation (APA)
Pantoji, S., van der Voort, M., McCarthy, S., Walle, C. J., Zattoni, G., Cruz, M., Kassapoglou, C., & Peeters, D. (2026). Generating realistic estimates of AFP tow geometry for gap and overlap predictions. *Composites Part A: Applied Science and Manufacturing*, *209*, Article 109984. https://doi.org/10.1016/j.compositesa.2026.109984

Important note
To cite this publication, please use the final published version (if applicable).
Please check the document version above.

Copyright
In case the licence states “Dutch Copyright Act (Article 25fa)”, this publication was made available Green Open Access via the TU Delft Institutional Repository pursuant to Dutch Copyright Act (Article 25fa, the Taverne amendment). This provision does not affect copyright ownership.
Unless copyright is transferred by contract or statute, it remains with the copyright holder.

Sharing and reuse
Other than for strictly personal use, it is not permitted to download, forward or distribute the text or part of it, without the consent of the author(s) and/or copyright holder(s), unless the work is under an open content license such as Creative Commons.

Takedown policy
Please contact us and provide details if you believe this document breaches copyrights.
We will remove access to the work immediately and investigate your claim.

This work is downloaded from Delft University of Technology.

Composites: Part A 209 (2026) 109984

Contents lists available at ScienceDirect

Composites Part A

journal homepage: www.elsevier.com/locate/compositesa

Generating realistic estimates of AFP tow geometry for gap and overlap predictions

Siddharth Pantoji [a], Martijn van der Voort [a], Seán McCarthy [a], Clifton-John Walle [a], Giovanni Zattoni [a], Manuel Cruz [a], Christos Kassapoglou [a], Daniël Peeters [a,b,*]

[a] Faculty of Aerospace Engineering, Delft University of Technology, Kluyverweg 1, Delft, 2629 HS, The Netherlands
[b] SAM XL - Smart Advanced Manufacturing, Rotterdamseweg 382c, 2629 HG Delft, The Netherlands

ARTICLE INFO

Dataset link: 4TU.ResearchData

MSC:
00-01
99-00

Keywords:
Gaps
Overlaps
Markov Chain Monte Carlo
AFP

ABSTRACT

Gap and overlap defects are formed during automated fiber placement (AFP) layup due to stochastic variations in tow position and geometry. There is utility in predicting the size and frequency of these defects since they affect the manufacturing rate and structural performance. Two methods which reflect the measured process variability were implemented to simulate realistic tow geometry. A Monte Carlo (MC) simulation used independent random sampling from the distributions of the sources of variation. A Markov Chain Monte Carlo (MCMC) simulation used the Random Walk Metropolis algorithm which samples these distributions while considering the neighborhood of past samples thus better preserving spatial continuity. Simulated tows were assembled into virtual laminae. Tow-level validation using spatial-frequency Fast Fourier Transform (FFT) analysis demonstrated that the MCMC method reproduces the dominant wavelengths and spectral characteristics of experimentally measured tow waviness, whereas the MC method introduces unrealistic high frequency variations. Lamina-level comparisons showed that while both methods predict similar gap and overlap area percentages, only the MCMC method accurately captures defect length distributions. The proposed framework provides realistic AFP layup geometries for use in mesoscale modeling and for informing process improvement efforts.

1. Introduction

Automated fiber placement (AFP) is a commonly used process for large composite part production and is expected to continue to be an attractive option. The runtime fraction of an AFP cell should be maximized to ensure high production rates. If one looks at the utilization time fractions of a real-world AFP cell, inspection and rework take up 35% of the time [1]. This cell down time is strongly linked to various types of AFP defects like gaps and overlaps which are the most numerous of all these AFP defects. It is advantageous to know the expected gaps and overlaps in a layup to balance the speed of manufacturing with allowable defect magnitude.

AFP manufacturing can involve layups with thermoset prepreg tow, thermoplastic tow or dry fiber tow, all of which lead to gap and/or overlap defects. These defects are expected to change shape during the later steps of manufacturing. They negatively affect structural performance depending on their severity and location [2,3]. Thus, knowing the layup geometry along with information about the size and frequency of gaps and overlaps is of interest for manufacturing process simulations and structural modeling of AFP composites.

In thermoset prepreg systems, several modeling efforts have focused on understanding how gaps close during autoclave processing. These models typically begin with a prescribed representation of the as-laid tow where the tow width, thickness and gap size are defined. Kermani et al. and Simacek et al. modeled gap filling using idealized unit-cell geometries, capturing squeeze flow, tow bending, and resin percolation mechanisms during consolidation [4,5]. Belnoue et al. and Jamora et al. embedded predefined gap and overlap features within meso-scale finite element models to study compaction behavior, thickness variation, and defect-induced waviness [6,7]. Thus, while the physical mechanisms governing defect evolution are modeled with increasing fidelity, the initial tow and defect geometries are prescribed deterministically.

For AFP layups with thermoplastic tow, follow-on processing steps may be designed to avoid the use of an autoclave. Niens et al. developed models to predict the in-plane permeability of thermoplastic preforms and the air evacuation time for vacuum bag only (VBO) processing of AFP preforms. These preforms were modeled to have a distribution of inter-tape channel dimensions informed by optical microscopy. The

* Corresponding author.
E-mail address: D.M.J.Peeters@TUDelft.nl (D. Peeters).

https://doi.org/10.1016/j.compositesa.2026.109984
Received 5 March 2026; Received in revised form 19 May 2026; Accepted 31 May 2026
Available online 12 June 2026
1359-835X/© 2026 The Authors. Published by Elsevier Ltd. This is an open access article under the CC BY license (http://creativecommons.org/licenses/by/4.0/).

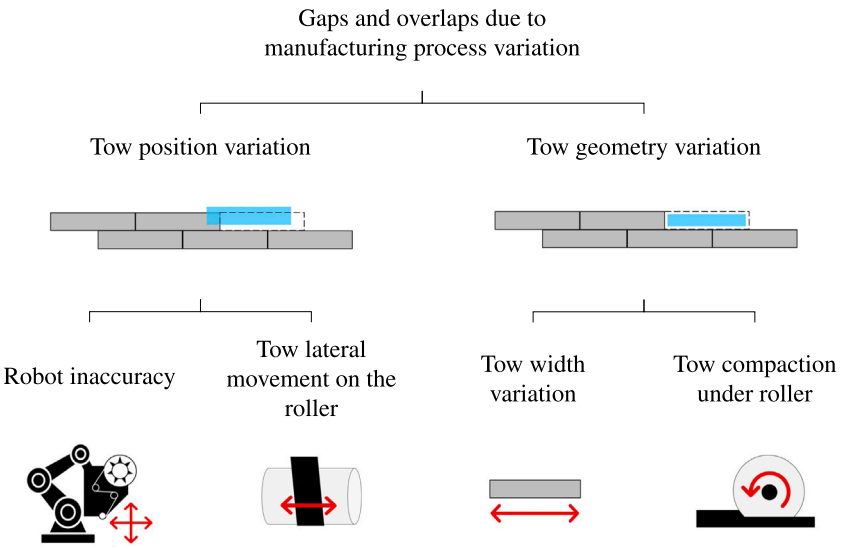


Fig. 1. Breakdown of the AFP manufacturing process variations which cause gap and overlap defects [19].

placement of these channels are fixed by the chosen layup stacking sequence. However, the geometric variability is introduced only through assigned channel dimensions without explicitly modeling their spatial variation along the channel [8]. Khaleghi et al. investigate consolidation behavior by intentionally programming gaps and overlaps of a certain magnitude and measuring the resulting void content in laminates using micro-CT scans. Their analysis is based on geometric configurations resulting from a few values of the programmed shift [9].

Across these studies involving both thermoset and thermoplastics materials, experimental measurements of tow morphology and gap size are often used to inform or validate models, but the generation of tow geometry itself is deterministic. Layup geometry details are prescribed using either idealized shapes or experiment informed shapes but they are not propagated into the model as a stochastic geometry input. If these process simulations are to be successfully applied to industrial AFP parts it would be necessary to have the accurate geometry descriptions of the AFP layup which are also representative of the spatial variability observed in real layups.

Structural models of AFP defects also require explicit defect geometries. Existing approaches include defect layers with degraded properties, sectional property assignment in gap/overlap regions, micrograph or CT informed geometries, prescribed half gap/half overlap trapezoidal features, and ply-by-ply meshing tools with specified gaps, overlaps, thickness variation, and waviness [2,10–16]. Across these approaches, the defect geometry is treated as a fixed input rather than as a stochastic outcome of tow placement variability.

Gaps and overlaps can be classified into two major categories – deterministic and stochastic – depending on their causes. The deterministic class of gaps and overlaps occur due to an inherent limitation in tow path generation for parts which have tows laid in non-geodesic paths. This occurs in flat parts manufactured by fiber steering or in doubly curved parts due to their geometry [17,18]. Tow paths are often generated by shifting a reference tow path in a given direction. Depending on the amount of shift, the part has either gaps, overlaps or a combination of both at locations which can be deterministically predicted when the layup is designed before manufacturing starts.

The stochastic category of gaps and overlaps occur due to manufacturing process variations. This class of defects are due to incorrect relative placement of the edges of adjacent tows. This placement can have 2 reasons: one, variation in positioning of the tow and, two, variation in geometry of the tow. This is illustrated in the schematics of Fig. 1 where the blue colored rectangle denotes the cross section of a tow being laid on the substrate. The figure also shows the further breakdown of these manufacturing process variations into possible sources.

Tow position variation could occur due to robot end effector path inaccuracy and lateral movement of the tow on the roller. Tow geometry variations could occur due to tow width and thickness variation of the incoming tow or due to tow deformation while being compacted by the roller [20]. These four variations can be measured by mounting various sensors to an AFP head during layup [21].

Various process and structural modeling efforts can benefit from accurate geometric layup information. In practice, AFP layups have gap and overlap defects due to manufacturing process variations which cannot be predicted before the layup. To the best of the author's knowledge, existing AFP tow and layup models prescribe geometry deterministically, using idealized or representative configurations rather than geometries reflecting process variability.

The objective of this work is to bridge this gap by using statistical descriptions of the manufacturing process variations to generate synthetic tow geometries and the resulting gap and overlap defects. By modeling tow geometry as a stochastic process, the proposed approach aims to produce virtual AFP layup geometries that are defect-equivalent to real laminates at the mesoscale level. Such representations can serve as realistic geometric inputs for downstream process simulations and structural analyses, enabling studies with higher fidelity.

2. Experimental dataset about manufacturing process variations in AFP

This study utilizes a previously published, publicly available dataset about manufacturing variations in AFP composites [22]. The experiment executed to create this dataset was designed to simultaneously measure the various sources of gap and overlap causing manufacturing variations during an AFP layup.

The experiment involved laying down nominally 6.35 mm wide unidirectional thermoset composite tow on a flat plate tool while recording tow position and tow geometry using various sensors. 31 straight 1 m lines of tow were laid. The AFP head positions recorded by the laser tracker were those of the achieved trajectory. The tow position on the compaction roller was measured using image processing on each recorded frame. The LLS A and LLS B are 2D profile sensors that record the tow geometry. As shown in Fig. 1, robot inaccuracy and lateral movement of the tow on the roller are causes of position variation while changes in tow width before and after compaction are causes of geometry variation.

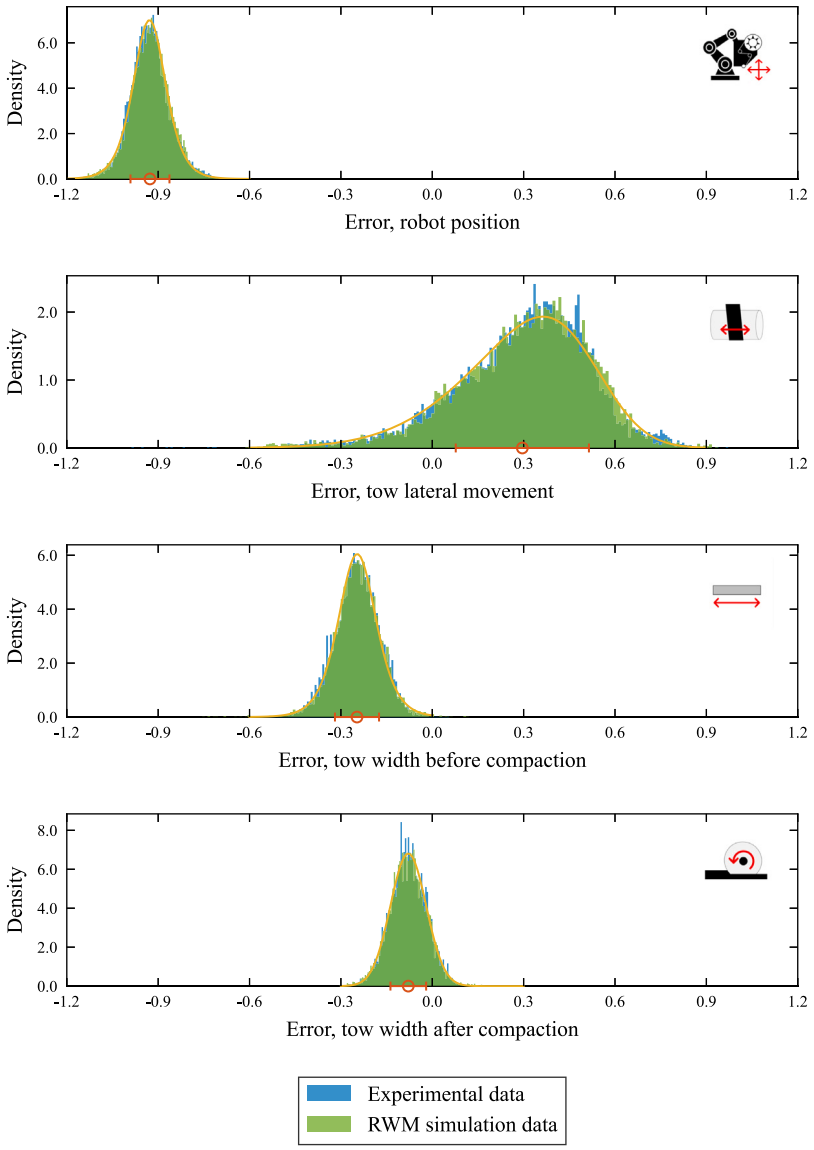


Fig. 2. (a–d top to bottom) Measured manufacturing variations that cause gaps and overlaps are shown in blue. Note that the X axis is equally scaled. Means and $\pm 1\sigma$ values are annotated in red. Distribution fits are annotated in yellow. Distributions from the random walk samples are shown in green.

Table 1
Summary of fits to distributions of measured manufacturing variations. Parameters are reported using the standard parameterization of each distribution - μ, s for the Logistic distribution, ξ, ω, α for the Skew-normal distribution and μ, σ for the Normal distribution.

	Robot inaccuracy	Tow lateral movement	Tow width variation	Tow width variation after compaction
Fit Type	Logistic	Skew Normal	Logistic	Normal
Location	$\mu = -0.93$	$\xi = 0.53$	$\mu = -0.25$	$\mu = -0.079$
Scale	$s = 0.036$	$\omega = 0.32$	$s = 0.041$	$\sigma = 0.058$
Shape	–	$\alpha = -2.29$	–	–

This resulted in the distributions for the four measured variations - robot inaccuracy, tow lateral movement on the roller, tow width before compaction and tow width after compaction. Fig. 2 shows these experimentally measured variations in blue color [19]. Fig. 2 also shows the fits in yellow. The fit parameters to these target distributions are listed in Table 1.

After the 31 lines of 1 m long tow were laid up, the layup was scanned with a laser line scanner (LLS). This resulted in geometry information of the laid tow and the resulting 30 gaps from the experiment. An example of an experimentally recorded tow can be seen in blue color in Fig. 3.

3. Simulation of AFP tows

A tow is represented by assembling sectional profiles along its length. Fig. 4 shows this representation. Linear interpolation is used between consecutive profiles. This is reasonable because adjacent profiles are closely spaced. Both the experimental and simulated tow

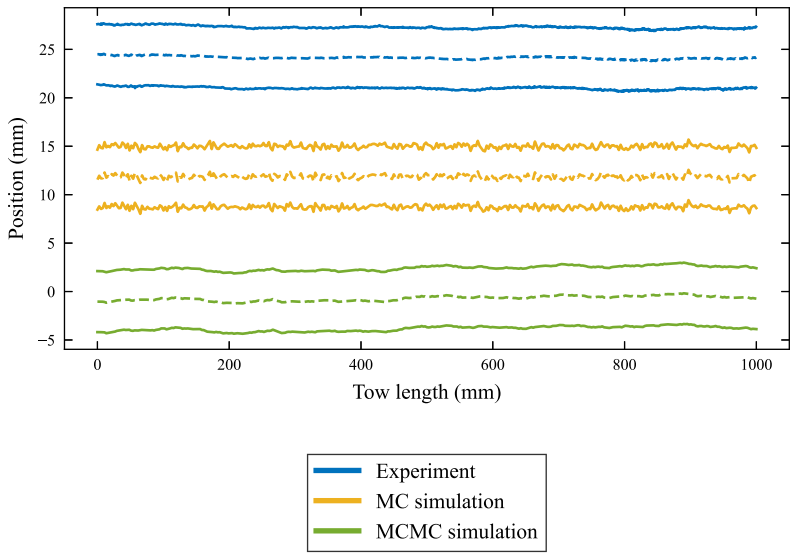


Fig. 3. Examples of experimentally measured tow (blue) along with synthetic tows simulated using the MC method (yellow) and the MCMC method (green).

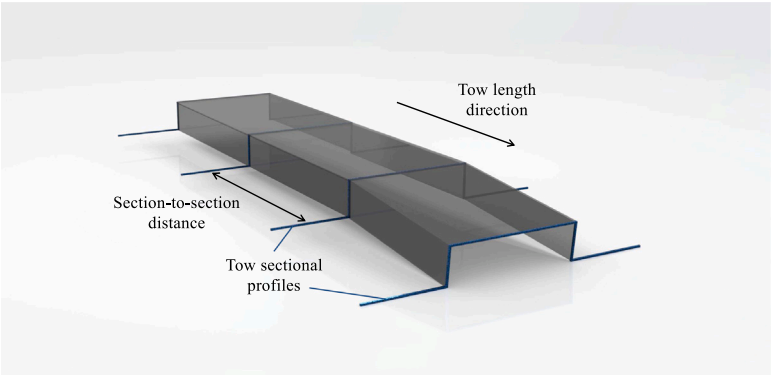


Fig. 4. Schematic showing the assembly of a representative tow from individual sectional profiles.

representations in this study have a lengthwise separation of less than 3 mm between the profiles. This study focuses on the profile geometry in the width direction since those lead to the formation of gaps and overlap defects.

Each tow profile is defined by tow position and geometry. The tow position determines the tow center line. The tow geometry determines the edges of the tow relative to the tow center. In this study the profile of the tow is simulated by sampling values related to the tow position and the tow geometry. The profiles are then stitched along the tow length, as shown in Fig. 4.

This section will compare two methods of creating synthetic tows. The first method uses Monte Carlo simulations based on random sampling. To overcome the shortcomings of this method, the second method uses Markov Chain Monte Carlo simulations with a sampling scheme based on the Random Walk Metropolis algorithm.

3.1. Tow simulation based on random sampling

The algorithm to simulate a tow section was as follows:

1. A position value is randomly sampled from the Logistic distribution in Fig. 2(a). This position value P_r describes the position of the AFP head/robot.

$$P_r \sim \text{Logistic}\,(\mu, s) \tag{1}$$

2. This was followed by the random sampling of another position value from the Skew Normal distribution seen in Fig. 2(b). This position value P_t describes the position of the tow on the roller.

$$P_t \sim \text{SkewNormal}\,(\xi, \omega, \alpha) \tag{2}$$

3. These two positions were added to get resultant tow position value. We now know the tow center position P_c for this simulation.

$$P_c = P_r + P_t \tag{3}$$

4. This is followed by a random tow width value sample W_a from the other Logistic distribution in Fig. 2(c).

$$W_a \sim \text{Logistic}\,(\mu, s) \tag{4}$$

Half of this tow width value is added and subtracted from the resultant position value to get the left edge $T_{L,a}$ and the right edge $T_{R,a}$ of the tow section.

$$T_{L,a} = P_c + \frac{1}{2}W_a, \qquad T_{R,a} = P_c - \frac{1}{2}W_a \tag{5}$$

5. This was followed by a random sampling of a value of the width after compaction from the Normal distribution seen in Fig. 2(d). It was made sure that this sample had a value greater than the value of the initial width sampled earlier. If not, resampling was done until this condition is satisfied. This condition ensured that

the tow section after compaction is always wider than the tow section before compaction.

$$W_b \sim \text{Normal}\,(\mu, \sigma \mid W_b \geq W_a) \tag{6}$$

6. The difference between the tow width after compaction and before compaction was used to pad the simulated tow width. Thus, the left edge $T_{L,b}$ and the right edge $T_{R,b}$ of the tow section after compaction are determined.

$$\Delta W = W_b - W_a \tag{7}$$

$$T_{L,b} = T_{L,a} + \frac{1}{2}\Delta W, \qquad T_{R,b} = T_{R,a} - \frac{1}{2}\Delta W \tag{8}$$

All the sampling steps in this algorithm were randomly implemented. The simulated tow was assembled by placing consecutive tow sections a fixed distance apart. This tow section to tow section distance was chosen as 2.65 mm. This value was based on the lowest frequency rate of the four data streams in the experimental dataset.

An example simulated tow made by this MC method of random sampling and assembly can be seen in Fig. 3 in yellow. It is visibly more wavy than the measured tow. This difference between the real tow and the simulated tow can be explained by the nature of the chosen sampling technique. The four experimental distributions for the four sources of variations – robot inaccuracy, tow lateral movement on the roller, tow width before compaction and tow width after compaction – are based on physical aspects of the material and the AFP layup process. When being recorded the values of these variations are changing continuously. However, in the tow section simulation algorithm, these values are sampled randomly. Therefore, tow position and geometry jump between sections, losing the continuity observed experimentally.

3.2. Tow simulation based on the Random Walk Metropolis algorithm

The shortcoming of significantly greater waviness in the tow has been overcome by using a sampling technique which bases current draws on the neighborhood of the past draw. This dependency on the past sampled value results in a sequence of values that forms a Markov chain.

This section details the implementation of a Markov Chain Monte Carlo simulation to create synthetic tows by using the Random Walk Metropolis algorithm [23]. In these tows, the consecutive samples are more likely to be close to each other due to the continuous variation of various aspects of the physical process.

The steps to create the tow section were similar to the steps described in Section 3.1 except that it simulated tow section width from samples of the tow width variation after compaction only. Tow width variation before compaction was neglected due to the inability to capture the width increase in the random walk chains. Thus, the simulation was implemented in the following steps with sampling for each source of variation except the width variation before compaction:

1. The target distribution $p(x)$ is the fit to experimental data described in Fig. 2. This target distribution is defined with θ_n which represents the various fitted parameters. The consecutively drawn samples need to eventually converge to these distributions.

$$p(x) = f(x \mid \theta_n) \tag{9}$$

The target distribution is Logistic for robot inaccuracy, Skew Normal for tow lateral movement and Normal for tow width after compaction. The parameters θ_n to these target distributions are listed in Table 1. These target distributions are seen in Fig. 2 in yellow.

2. The algorithm involves proposing a new value x^* when the current value is x_0. This proposal x^* is a sample from the symmetrical proposal distribution. This proposal distribution was selected to be a Gaussian distribution centered at the current value. Thus the proposed value will be given by

$$x^* \sim \mathcal{N}(x_0, \sigma^2) \tag{10}$$

The standard deviation of the Gaussian proposal distribution is chosen to match the experimentally observed variability between consecutive measurements of the same process variable, thereby ensuring that the random walk reproduces the physically realistic step-to-step continuity of the AFP process. Thus, if x_i is the experimentally measured sequence of a given process variation, the standard deviation of the proposal distribution is chosen as

$$\sigma = \text{std}(x_{i+1} - x_i) \tag{11}$$

3. The acceptance ratio is calculated as

$$\alpha = \min\left(1, \frac{p(x^*)}{p(x_0)}\right) \tag{12}$$

where $p(x^*)$ and $p(x_0)$ are the values of the probability density function of the target distribution for the proposed value and the current value of the Markov chain.

4. The proposed new value x^* is accepted or rejected according to an acceptance rule. The acceptance rule is based on the comparison of α with a random sample from a uniform distribution of numbers between 0 and 1.

$$x_1 = \begin{cases} x^*, & \text{if } U \leq \alpha, \quad U \sim \mathcal{U}(0,1) \\ x_0, & \text{otherwise.} \end{cases} \tag{13}$$

5. The above proposals along with acceptances/rejections are implemented iteratively to achieve a chain of samples $\{x_n\}$ whose stationary distribution corresponds to the target probability density of the relevant source of variation.

The Markov chain was initialized randomly within the experimentally measured range of each variation, so only a minimal burn-in or converging period was required. Because the Gaussian proposal distribution is centered at the current value, proposed moves are local, with σ controlling the neighborhood size. This prevents unrealistic value jumps as seen in the Monte Carlo simulations described in Section 3.1. Moves towards significantly lower density regions are rarely accepted while moves towards moderately lower density are accepted relatively frequently. The chain spends time in various regions in a way which is proportional to the target density. Over time it converges to the target distribution.

The distributions of the RWM samples for the respective sources of variation are annotated in green in Fig. 2. These distributions are constructed from the full set of samples generated during the 31 simulated tows, corresponding to the 31 experimentally measured tows. They correspond well to the respective target probability densities annotated in yellow. Table 2 gives the comparison of the mean and spreads of the distributions formed by the samples of the simulated Markov chains to those measured experimentally. The close agreements in these statistics signify good convergence of the random walk simulation.

The consecutive tow sections are simulated using these RWM samples and assembled into a tow representation which has its position and geometry varying realistically. An example simulated tow made by this MCMC method is seen in Fig. 3. The lines in this MCMC simulated tow (green) oscillate with much lower frequency and look much more similar to the physical tows from an AFP layup (blue) compared to the example simulated tow made by the MC method (yellow).

In the MC method, the samples were random and independent. Hence the tow simulation could ensure that width after compaction is greater than the width before compaction. New values were sampled until this condition was met. The MCMC method leads to a chain of variation values which are dependent on the past values. Therefore, the section simulations can occur when the value of the chain of width

Table 2
Comparison of the distributions of the four sources of variations derived from the model and the experimental layup.

		Robot inaccuracy	Tow lateral movement	Tow width variation	Tow width variation after compaction
Experiment	Mean (mm)	−0.93	0.30	−0.25	−0.08
	Standard deviation (mm)	0.06	0.22	0.07	0.06
Random Walk algorithm	Mean (mm)	−0.93	0.29	−0.25	−0.08
	Standard deviation (mm)	0.06	0.22	0.07	0.06

variations and width variations after compaction are such that the condition of width after compaction being greater than width before compaction is not met. This condition was not met, causing a non-physical width decrease in 3.9% of the sections. Therefore, the MCMC simulation was implemented without considering the effect of width before compaction. Future work can look into an advanced version of this Random Walk sampling which samples simultaneously from the width variation distribution and the width variation after compaction distribution while enforcing that the two chains are strictly kept away from directions which lead to the non-physical tow width decrease.

While the virtual laminae in this study can be stacked up to create a laminate, it neglects the out-of-plane waviness of the tow laid on a defect. Future work can investigate simple out-of-plane waviness shape descriptors and rules to capture how these defects stack up over multiple laminae.

4. Validation

The MCMC simulated tow in Fig. 3 looks more representative of the experimentally measured tow than the MC simulated tow. This visual similarity needs to be validated with quantitative and qualitative metrics to ensure that the virtual laminate with synthetic tows has a similar number and size of defects as those which would be seen in a real AFP laminate with physical tows.

For the purpose of validation, the simulated tow needs to be compared with an experimental tow to examine if it is equivalent in terms of the variations seen in the tow position and tow geometry. By extension, this equivalency would also mean that the magnitude and frequency of the gaps and overlaps will be comparable. Thus, the validation is performed at two levels, once by comparing experimental tow with the synthetic tow and then by comparing the experimental lamina with a virtual lamina.

4.1. Tow level comparison

The edges of the simulated tow are observed to have spatial waviness over a range of length scales. The resulting centerline of this simulated tow consequently has some spatial waviness characteristics. This can be compared to the spatial waviness characteristics of the centerline of the experimentally measured tow. Such comparisons can be achieved using a Fast Fourier Transform (FFT) on the spatial signal of the tow centerlines, yielding spatial-frequency amplitude spectra. These spectra describe how the magnitude of centerline variation is spread across spatial frequencies thus providing insight into the spatial correlation of the experimental and simulated tow centerlines. The spectral comparisons can be made using physical interpretations of metrics like spectral magnitude which reflects how large the tow centerline deviations are in amplitude and the dominant spatial frequencies which reflects the distances over which the tow oscillates along its length.

The spatial signals were interpolated onto a uniform spatial grid prior to spectral analysis to satisfy FFT sampling requirements. Fig. 5 shows representative examples of spatial-frequency amplitude spectra of the centerline variations of an MC simulated tow, an MCMC simulated tow and an experimental tow. Fig. 5(a) shows that in all cases, the spectra are dominated by low spatial frequencies, indicating that the tows primarily exhibit long-wavelength undulations. The Y axis of the figure was truncated to aid clarity of the lower amplitude regions. The MCMC tow spectrum exhibits significantly better agreement with the experimental tow spectrum in both amplitude and decay behavior across the low-frequency and mid-frequency ranges, whereas the MC tow spectrum significantly underpredicts low frequency content. At higher spatial frequencies, all spectra converge towards a low-amplitude experimental noise level.

The long-wavelength offset components of the tow centerlines reflect the global waviness behavior during AFP layup and represent relevant, physically meaningful features of the tow geometry. However, they dominate the raw FFT magnitude and could obscure shorter wavelength features. To examine shorter wavelength features in greater detail, standard preprocessing steps including linear detrending, windowing, and zero-padding were applied, resulting in the spectra seen in Fig. 5(b). The linear detrending removed the offset component and average slope of the centerline. The windowing introduced minimal end-tapering to reduce spectral leakage from discontinuities at the start and the end of the signal. These discontinuities exist because the tow start and end positions can be at non-zero values. The signals were then zero-padded prior to FFT evaluation to provide finer frequency binning for visualization and comparison. The spectra in Fig. 5(b) also show similar spectral shape and comparable spectral magnitude between MCMC simulation and experimental tow. The MC simulated tow displays broadband amplitudes across the frequency range, showing weak spatial correlation with the experimental tow.

Quantitatively, the average Pearson spectral correlation coefficient for the MCMC simulated tows was $\rho = 0.752$, indicating good agreement in spectral shape with the experimental tow. For the MC simulated tows it was $\rho = -0.027$, indicating negligible correlation. The average dominant spatial frequency was 2.1 cycles/m for the experimental tows, 2.7 cycles/m for the MCMC tows and 133.3 cycles/m for the MC tows. The MCMC tows match closely to the long-wavelength regime observed experimentally while the MC tows show much higher and noisier dominant frequencies.

All together, these qualitative and quantitative comparisons demonstrate that the MCMC method more effectively reproduces the spatial correlation structure, dominant frequencies, and overall magnitude of experimental tow waviness than the MC approach.

4.2. Lamina level comparisons

Several simulated tows can be assembled with the appropriate offsets to create a virtual lamina. Fig. 6 shows an example virtual lamina constructed using the MCMC method. It shows the resulting gaps and overlaps in white and dark gray respectively. These resulting defects depend on the waviness of the tow edges and on the offsets i.e. how far apart they are laid adjacently. The programmed shift for this virtual lamina was one tow width equivalent i.e. 6.35 mm. The experimental layup had a programmed shift of 12.5 mm. For purposes of the comparison, this experimental data was normalized by shifting them in the width direction to have a programmed shift of one tow width. This normalization assumes that the edge interactions in areas of the overlap do not affect its magnitude. It also assumes that the robot inaccuracy is similar for the supposed trajectory at the normalized shift.

A virtual lamina of 31 tows was constructed to compare it to the similarly laid experimental lamina with an equal number of tows

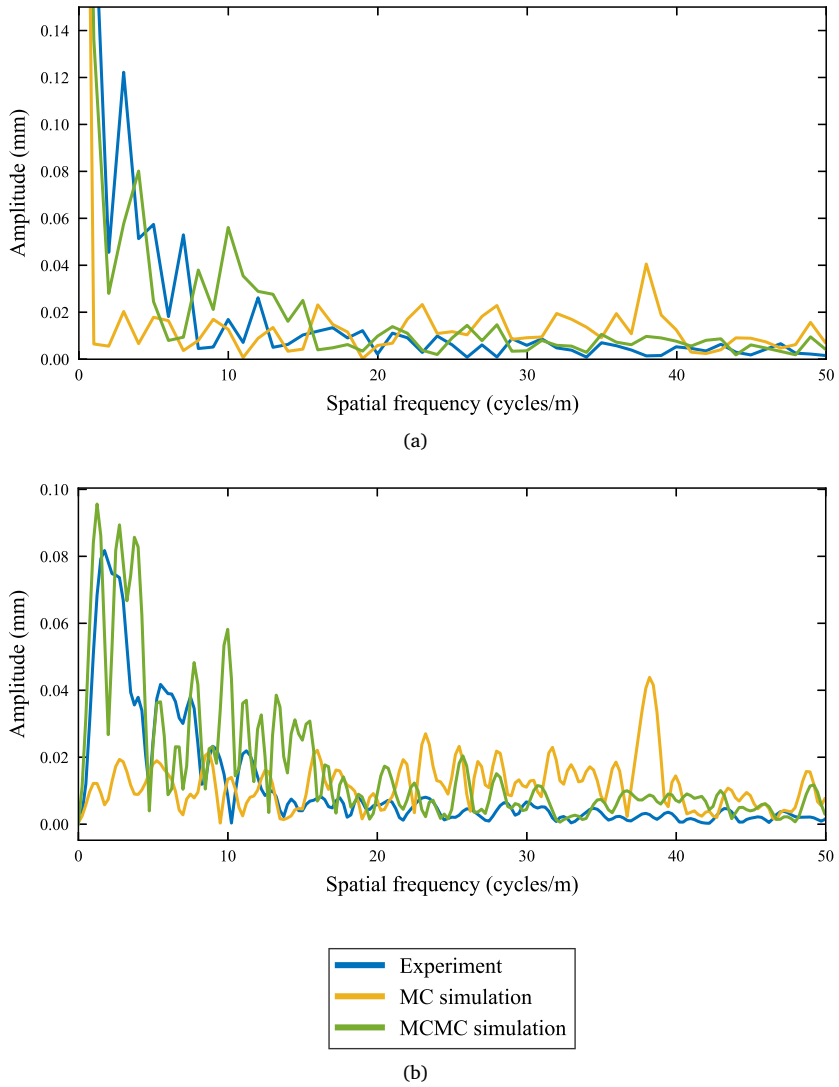


Fig. 5. FFT analysis of tow centerlines of example simulated tows and an experimental tow. The top figure (a) shows the resulting spectra for FFT of the tow centerlines without any additional processing. The bottom figure (b) shows the resulting spectra for FFT of the tow centerlines after processing steps like detrending, windowing and padding.

to compare the occurrence of gaps. Fig. 7 shows the distribution of experimentally measured gaps in blue. The gaps from the MCMC virtual lamina are depicted in green while the gaps from the MC virtual lamina are depicted in yellow. The gaps from the virtual lamina created using the MCMC method quantitatively match more closely with the experimentally measured gaps than the gaps from the MC method. The location of the gap distributions align well for both the models. The experimental distribution and simulated distributions of gaps are summarized in Table 3. The small quantitative mismatch may be related to possible cross-correlations between the four sources of variation. For example, when a robot path deviation takes place, it may not influence the tow deviation on the roller. In this case, the tow lateral movement will be recorded in addition to the robot inaccuracy, even when the tow is being appropriately laid. The simulation method ignores these potential interactions and assumes the four sources are independent.

Another comparison between the two simulation methods is done by measuring the defect area. The percentage area of gaps and overlaps in the normalized experimental layup was calculated to be 2.73% and 1.28%. A virtual lamina with an equal number of tows was generated numerous times using both MCMC and MC methods and the average percentage of gaps and overlaps was calculated. These results from both the methods are summarized in Table 4 and show good correlation.

The comparison of model performance using the distribution of defects or the defect area percentage in the earlier paragraphs lacked information on the continuity of gaps. The distribution or the percentage area of defects do not have a one-to-one conversion to the length of the defects. Thus it is essential to compare the lengths of the defects formed in the virtual lamina and the experimental lamina as seen in Fig. 8. It can be observed that the MC method overestimates the number of smaller gaps and also completely misses the higher gap lengths. The MCMC method estimate of the length of defects is much more closely correlated to the experimentally measured lamina.

To summarize, the various comparisons between the two methods of simulation and the experimental data have shown that the defect distribution or area can be acceptably predicted by both the MC and MCMC simulation methods. However, the MCMC method simulates tows and laminae which are representative in not just the defect frequency and defect magnitude but also in the length of defects found in real laminae. The neighborhood sampling used in the MCMC method leads

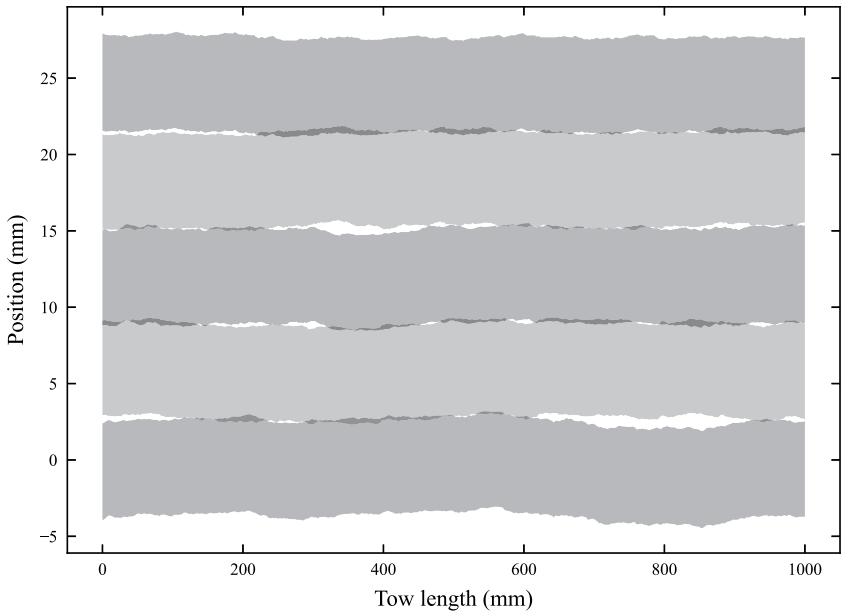


Fig. 6. Example virtual lamina simulated using the MCMC method.

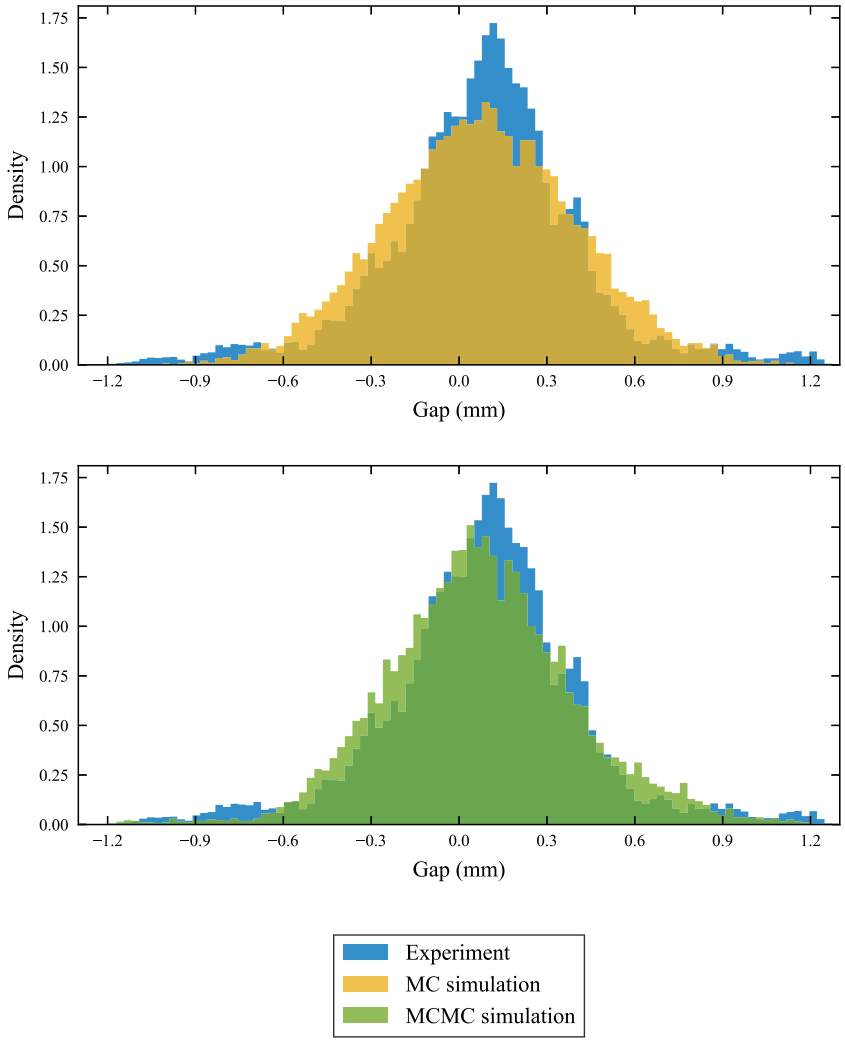


Fig. 7. A, B (top, bottom). Comparison of predicted gaps and experimentally measured gaps. Gaps predicted using MC simulations are shown in yellow. Gaps predicted using MCMC simulations are shown in green. Experimentally measured gaps are shown in blue.

Table 3
Comparison of the distribution of predicted gaps for the MC and MCMC method with the distribution of experimentally measured gaps.

		Mean (mm)	Standard deviation (mm)	90th percentile (mm)	99th percentile (mm)
Measured gaps		6.24	0.34	6.59	7.25
Predicted gaps	MC simulation	6.22	0.32	6.64	6.99
	MCMC simulation	6.22	0.32	6.62	7.04

Table 4
Comparison of predicted gap and overlap defect area for the MC and MCMC method with experimentally measured gap and overlap defect area.

		Gaps % area	Overlaps % area
Experimental layup		2.73	1.28
Virtual lamina	MC simulation	2.60	1.48
	MCMC simulation	2.77	1.58

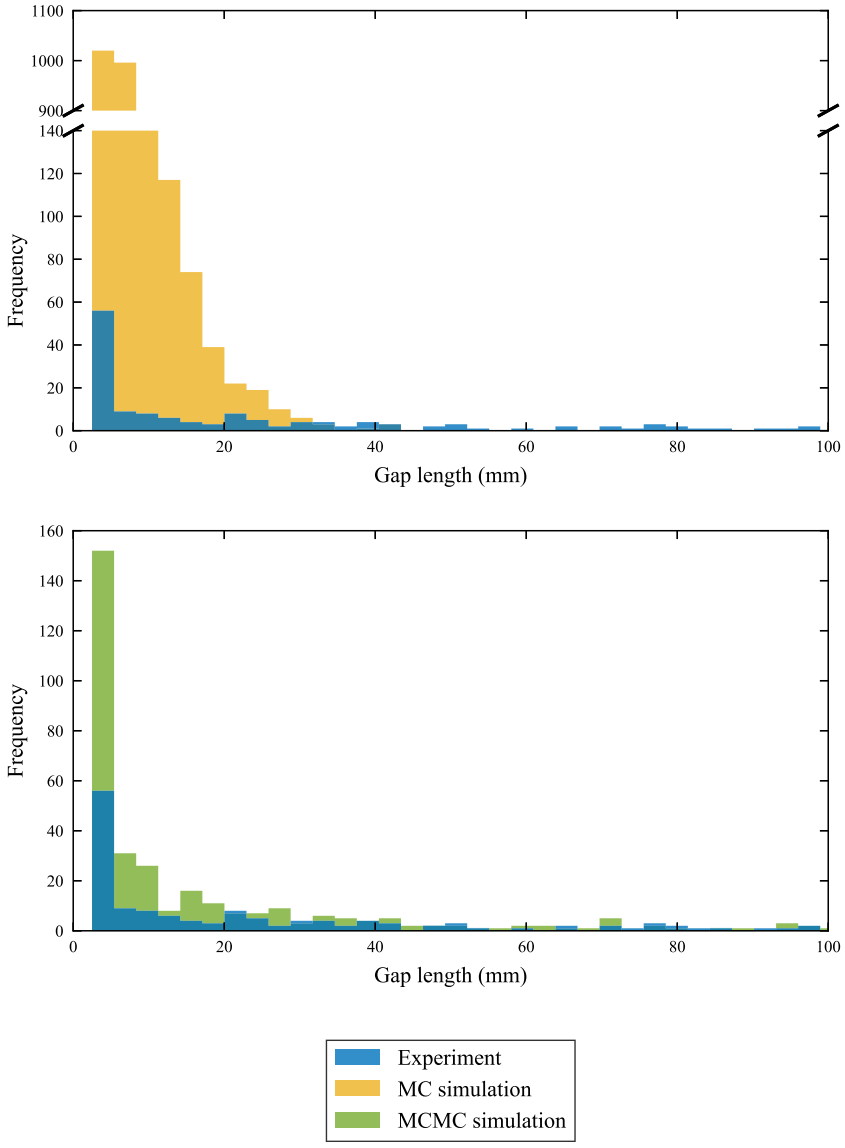


Fig. 8. Comparison of the distributions of length of defects between the experimental lamina and the simulated lamina.

to position and geometry samples which vary continuously, similar to the physical phenomenon they are based on. Owing to this sampling method where each sample is informed by the past sample, the MCMC method can be used to simulate tows and construct virtual laminae which are similar to real layups.

The framework was informed by parametric fits to the distributions obtained by experimental measurements during layup. However, the comparisons were made with separate post-layup measurements of the same campaign. Thus, this validation comes with the limitation that the comparisons were not against an independent campaign.

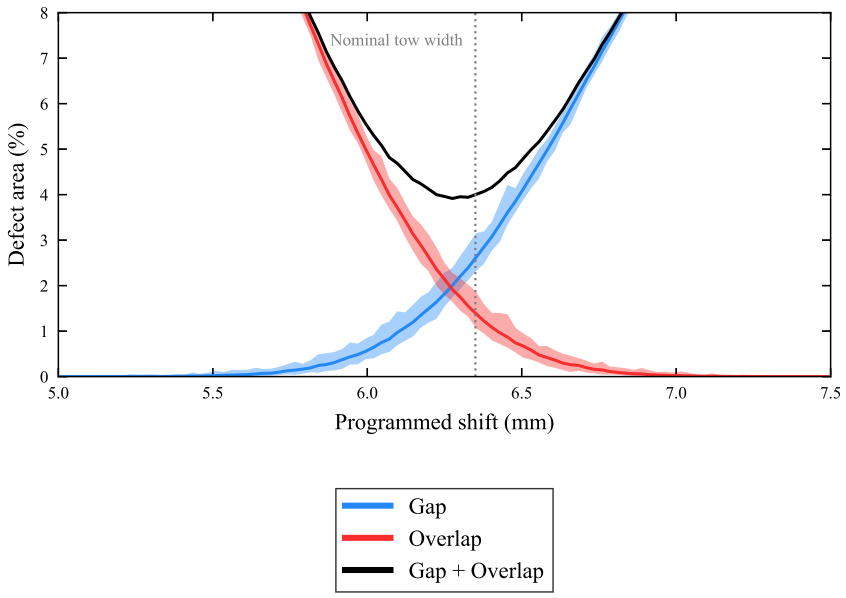


Fig. 9. Illustration of optimal programmed shift for minimizing defect area percentage. The variation bands on the gap and overlap lines show the stochasticity of the defect population.

5. Utility for AFP technology and process design

In addition to the uses mentioned in the introduction, simulated tows and the resulting virtual laminae can also provide insights into AFP technology and process improvements. The analyses presented in this section are enabled by the statistical description of the four sources of AFP manufacturing variation considered in this study. These input distributions are specific to the AFP machine, tow material, process parameters and the geometry of the manufactured part. They are obtained by measuring a representative set of manufactured tows. Once available, they allow for the evaluation of the gap and overlap defect populations corresponding to the manufacturing conditions under which the representative data were collected. While the results reported here are therefore specific to the described experiment, the methodology itself is directly applicable to other scenarios provided the corresponding statistical inputs are obtained.

5.1. Optimal programmed shift

The programmed shift or (interband) offset is the distance between planned paths of adjacent tows or courses of an AFP layup. This programmed shift between adjacent tows needs to be minimized to reduce gaps. This is because gaps are associated with structural performance knockdowns. However, decreasing the programmed shift has the effect of increasing the probability of overlap defects. Overlap defects during the layup need repair and rework thus slowing down the process and leading to higher manufacturing costs. Thus the programmed shift is a balance between the mechanical knockdowns from gap defects and the additional manufacturing process cost due to overlap defects.

The MCMC method was used to simulate laminae with various values of the programmed shift. This resulted in the values of gap and overlap defect areas for a range of programmed shift values as plotted in Fig. 9 in red and blue. It shows the increase in gap area percentage as the programmed shift increases and the increase in overlap area percentage as the programmed shift decreases. The optimal programmed shift at which the total defect area is minimized is 6.27 mm. This plot can be modified to weigh the gap and overlap curves with associated costs. The gap curve can be weighted for mechanical knockdown costs while the overlap curve can be weighted for process costs with rework. Optimization of the weighted defect curves would yield an optimal programmed shift. Thus, the developed simulation methods could be useful for a tradeoff analysis between gaps and overlaps. The simulation could be used for programmed shift value selection before qualification and thus can help reduce expensive prototype iterations.

The stochasticity in each simulation leads to slight variation in the defect area percentage of each simulated lamina. The simulations were run a 100 times for each value of the programmed shift to find the statistical variation in the gap and overlap defect area. The bounds of this variation are annotated in Fig. 9 as light blue and light red color bands. Thus, these MCMC simulations statistically relate AFP process parameters to defect population characteristics and scatter. This information can be useful for certification activities such as establishing manufacturing allowables. It would reduce conservatism in manufacturing process design which is often driven by uncertainty in worst-case defect scenarios and stacking effects, particularly in structurally critical regions of the airframe.

5.2. Prioritizing of AFP process improvements using uncertainty propagation

There are various technological ways to reduce the manufacturing process variations in AFP layups. The robot accuracy can be improved by installing secondary feedback loops or newer robot models with higher path accuracy. The AFP feed system can be improved to reduce the tow lateral movement. The tow material dimensional tolerance specifications can be made tighter. Each of these process improvements entails different costs. Thus knowing the effectiveness of these measures in laminate quality will be useful in prioritizing these measures for layup quality improvements.

Fig. 10 shows the gap and overlap area percentages in laminae when eliminating the various sources of variations one at a time. This figure was created by simulating laminae a 100 times for each elimination. For the chosen AFP head, material system and process conditions, the gap defect percentage will be reduced by 47%, 4% and 1% when tape lateral movement, robot inaccuracy and width variations are eliminated, respectively. Eliminating position variations of the tow lateral movement will lead to a higher improvement in laminate defects than eliminating geometry variations of the tow width.

Fig. 10 resulted from running the simulations with stochastic inputs based on the fits to the four measured sources of variations in the experimental campaign. But more generic simulations can be executed to understand the behavior of this statistical framework which describes

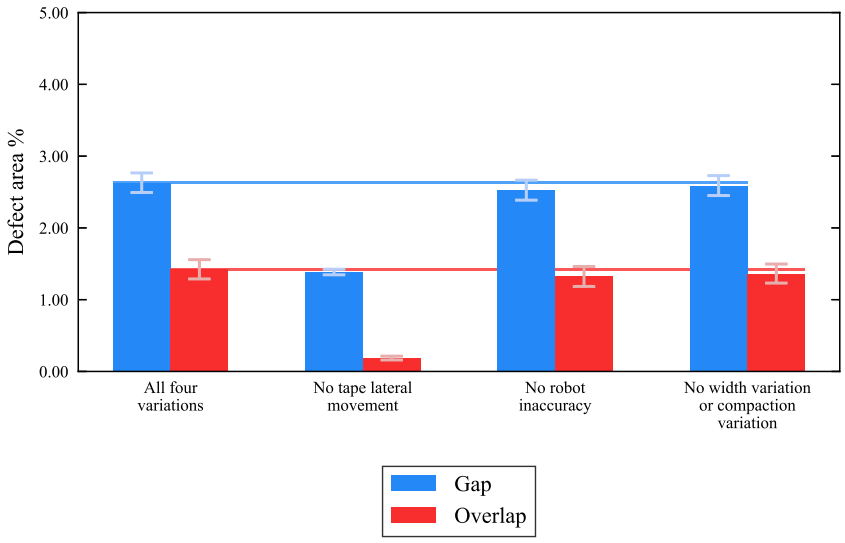


Fig. 10. Defect area percentage when variations from the various sources of variations are eliminated one at a time.

Table 5
Propagation of input distribution perturbations through the MCMC simulation to the resulting defect distribution. The increased input values of μ and σ were 0.5 mm and 0.15 mm, respectively, compared with baseline values of 0 mm and 0.1 mm. Stochastic noise is present in the reported values. PV = position variation; GV = geometry variation; * = obtained using MC simulation.

No.	Input variations	Output defect distribution		Comments
		μ (mm)	σ (mm)	
1	All four inputs with $\mu = 0$ and $\sigma = 0.1$	0.0003	0.2123	Baseline simulation
2	Higher μ for one PV	0.0005	0.2121	Negligible effect
3	Higher σ for one PV	−0.0012	0.2656	25% increase in defect spread
4	Higher σ for both PVs	0.0001	0.3058	44% increase in defect spread
5	Higher μ for one GV	−0.5002	0.2113	Shift in defect mean towards overlap region
6	Higher μ for both GVs	−0.5819	0.2083	Shift in defect mean towards overlap region*
7	Higher σ for one GV	0.0015	0.2271	7% increase in defect spread
8	Higher μ and σ for PVs and GVs	−0.6230	0.3121	Combined worst case scenario*

the AFP process. For these generic simulations, the four stochastic inputs were represented using normal distributions. Normal distributions were selected because they are widely used parametric descriptions of manufacturing variability. Moreover, the focus is on the propagation behavior of the framework rather than the input variation characteristics. The mean and standard deviation were chosen to be 0 mm and 0.1 mm respectively for the baseline simulation. Input variations were individually perturbed to higher values and were then compared with the baseline simulation to understand their effects on the defect population. The higher values for the mean and standard deviation were chosen to be 0.5 mm and 0.15 mm respectively. The various mean and standard deviation values were chosen to be comparable to the experimentally observed values. The changes in mean would represent a process bias such as average tow width being offset from the specified width, or tow lateral movement which is biased to one side of the roller center due to reasons like roller wear and bearing misalignment. The changes in standard deviations represent the control on the spread of the geometry or position variables such as tape slitting width changes or robotic path variation in various sections of the workspace. The results of the generic simulations for various uncertainty scenarios are briefly summarized in Table 5. They have been compared to the resulting defect distribution from the baseline simulation which had a mean of 0 mm and a standard deviation of 0.21 mm.

It was found that changing the mean of any of the position variations had negligible effect on the defect magnitude distributions. This was due to the collective shifting of all the tows rather than relative to each other. However, increasing the standard deviation of one or both positional variations to 0.15 mm increased the output standard deviation by 25% and 44%, respectively, relative to the baseline. Thus, the spread in the position variations is not an additive effect. The two position variations interact and propagate non-linearly.

When the mean of the geometry variation from the width after compaction was increased to a value of 0.5 mm, this caused many more overlaps than gaps, thus shifting the mean of the defect magnitude distribution to −0.5 mm. When both the geometry variations had an increased mean value of 0.5 mm, the shifting of the mean of the defect magnitude distribution towards the overlap direction was greater at −0.58 mm. Thus, the combined effect was not additive. When the standard deviation of the geometry variation from the width after compaction was increased to 0.15 mm, the standard deviation of the defect magnitude distribution increased slightly by 7%. A minor further increase was seen in the standard deviation of the defect magnitude distribution when the standard deviation of both the geometry variations was increased.

If the mean and the standard deviations were increased for all the variations, representing a hypothetical worst case scenario, the standard deviation of the defect magnitude distribution increased by 50%. Overall, position variations primarily broadened the defect distributions while a systemic bias in geometry variations mainly shifts the mean of the defect distributions in opposite directions of the bias.

Thus, this framework can be used to implement an uncertainty propagation study to provide such quantitative and qualitative insight about how the individual inputs propagate via the AFP manufacturing process to affect the defect population characteristics. Another effect captured by the simulation framework is the relative effects of position variations and geometry variations in the formation of gap and overlap defects on either side of the tow. Variations of the same magnitude produce substantially greater edge waviness when arising from position variations rather than geometry variations.

6. Conclusion

This study demonstrates that the proposed framework can use statistical data about the sources of AFP manufacturing variations to construct realistic synthetic tows and virtual laminae which reproduce experimentally observed gap and overlap defect characteristics.

Two methods to simulate the tow were implemented and evaluated — Monte Carlo (MC) simulations and Markov Chain Monte Carlo (MCMC) simulations. Tows created using the MC simulations had more waviness compared to the observations of real AFP laid tows. This was attributed to the random sampling which led to variation values which jumped drastically across the distributions rather than following continuous changes like the physical process they describe. This limitation was improved upon in the MCMC simulations which used the Random Walk Metropolis (RWM) method for sampling. This led to simulated tows whose waviness is more realistic than the simulated tows created by random sampling.

The validation efforts for these two methods were done on the tow level and the lamina level. On the tow level, an FFT analysis of the tow centerlines showed spatial-frequency amplitude spectra with acceptable correlation between the experimental tow and the MCMC simulated tow. The MC simulated tow did not match the dominant spatial amplitudes seen in experimental tows. On the lamina level, the gap distributions and the gap area percentage yielded close values for both the MCMC and the MC simulations. However, the MC method led to a simulated lamina with a high number of shorter gaps and no longer gaps. It lacked a match with the experimental observations of the length of defects. The MCMC method led to a closer match with the experimental observations across shorter and longer length of defects. These comparisons also showed that the virtual and experimental lamina equivalence must be established in the frequency, magnitude and the length of gap and overlap defects.

Though the motivation of this study was to create realistic virtual AFP composite layup descriptions for application in structural and process modeling, other uses related to optimal process design were identified. The virtual laminae can be used to identify the optimum programmed shift in adjacent tows to achieve the right balance of gaps and overlaps. Another use of these simulation methods which are informed by manufacturing variation data is in prioritizing the process improvements required in tightening the AFP layup to the needed levels of quality.

CRediT authorship contribution statement

Siddharth Pantoji: Writing – original draft, Validation, Supervision, Methodology, Investigation, Data curation, Conceptualization. **Martijn van der Voort:** Visualization, Software, Methodology, Formal analysis, Conceptualization. **Seán McCarthy:** Visualization, Software, Methodology, Formal analysis, Conceptualization. **Clifton-John Walle:** Visualization, Software, Methodology, Formal analysis, Conceptualization. **Giovanni Zattoni:** Visualization, Software, Methodology, Formal analysis, Conceptualization. **Manuel Cruz:** Visualization, Software, Methodology, Formal analysis, Conceptualization. **Christos Kassapoglou:** Writing – review & editing. **Daniël Peeters:** Writing – review & editing.

Declaration of competing interest

The authors declare that they have no known competing financial interests or personal relationships that could have appeared to influence the work reported in this paper.

Acknowledgments

The authors would like to thank Diogo Ying for his contributions towards CAD development and preliminary modeling efforts, and Taran Kalma, Johannes Nilsson, Théotime Pinchart and Sam Rotteveel for their involvement in the initial course-based project phase.

Data availability

Raw data from the mentioned experiment is available on the 4TU.ResearchData repository.

References

[1] Rudberg T, Nielson J, Henscheid M, Cemenska J. Improving AFP Cell Performance. SAE Int J Aerosp 2014;7(2):317–21. http://dx.doi.org/10.4271/2014-01-2272.

[2] Del Rossi D, Cadran V, Thakur P, Palardy-Sim M, Lapalme M, Lessard L. Experimental investigation of the effect of half gap/half overlap defects on the strength of composite structures fabricated using automated fibre placement (AFP). Compos Part A: Appl Sci Manuf 2021;150(May):106610. http://dx.doi.org/10.1016/j.compositesa.2021.106610.

[3] Croft K, Lessard L, Pasini D, Hojjati M, Chen J, Yousefpour A. Experimental study of the effect of automated fiber placement induced defects on performance of composite laminates. Compos Part A: Appl Sci Manuf 2011;42(5):484–91. http://dx.doi.org/10.1016/j.compositesa.2011.01.007.

[4] Niknafs Kermani N, Gargitter V, Simacek P, Advani SG. Gap filling mechanisms during the thin ply Automated Tape Placement process. Compos Part A: Appl Sci Manuf 2021;147(April):106454. http://dx.doi.org/10.1016/j.compositesa.2021.106454.

[5] Simacek P, Niknafs Kermani N, Gargitter V, Advani SG. Role of resin percolation in gap filling mechanisms during the thin ply thermosetting automated tape placement process. Compos Part A: Appl Sci Manuf 2022;152(September 2021):106677. http://dx.doi.org/10.1016/j.compositesa.2021.106677.

[6] Belnoue JP, Mesogitis T, Nixon-Pearson OJ, Kratz J, Ivanov DS, Partridge IK, Potter KD, Hallett SR. Understanding and predicting defect formation in automated fibre placement pre-preg laminates. Compos Part A: Appl Sci Manuf 2017;102:196–206. http://dx.doi.org/10.1016/j.compositesa.2017.08.008.

[7] Jamora VC, Rauch V, Kravchenko SG, Kravchenko OG. Effect of Resin Bleed Out on Compaction Behavior of the Fiber Tow Gap Region during Automated Fiber Placement Manufacturing. Polymers 2024;16(1). http://dx.doi.org/10.3390/polym16010031.

[8] Niens L, Swamy J, Grouve W, Wijskamp S, Akkerman R. Prediction of the in-plane permeability and air evacuation time of fiber-placed thermoplastic composite preforms with engineered intertape channels. Compos Part C: Open Access 2024;14(April):100475. http://dx.doi.org/10.1016/j.jcomc.2024.100475.

[9] Khaleghi S, Kirchhoff JG, Pandher J, Lacalle J, Tehrani M. Efficient consolidation of thermoplastic composites using AFP-engineered air channels and optimized VBO processing. Compos Part B: Eng 2026;310:113134. http://dx.doi.org/10.1016/j.compositesb.2025.113134, URL https://www.sciencedirect.com/science/article/pii/S1359836825010509.

[10] Fayazbakhsh K, Arian Nik M, Pasini D, Lessard L. Defect layer method to capture effect of gaps and overlaps in variable stiffness laminates made by Automated Fiber Placement. Compos Struct 2013;97:245–51. http://dx.doi.org/10.1016/j.compstruct.2012.10.031.

[11] Experimental and numerical investigation on the open-hole compressive strength of AFP composites containing gaps and overlaps. J Compos Mater 2017;51(26):3631–46. http://dx.doi.org/10.1177/0021998317690917.

[12] Sawicki AJ, Minguet PJ. Effect of intraply overlaps and gaps upon the compression strength of composite laminates. Collect Tech Pap - AIAA/ASME/ASCE/AHS/ASC Struct Struct Dyn Mater Conf 1998;1:744–54. http://dx.doi.org/10.2514/6.1998-1786.

[13] Rossi DD. effect of half gap/overlap defects on the strength of composite structures fabricated with automated fiber placement methods [Ph.D. thesis], McGill University; 2019.

[14] Diemar F, Holmes J, Sommacal S, Aparici-Böhlke D, Böckl B, Drechsler K, Compston P. X-ray micro-computed tomography for mechanical behaviour analysis of Automated Fiber Placement (AFP) laminates with integrated gaps and overlaps. Compos Struct 2025;351(June 2024):118601. http://dx.doi.org/10.1016/j.compstruct.2024.118601.

[15] Li X, Hallett SR, Wisnom MR. Modelling the effect of gaps and overlaps in automated fibre placement (AFP)-manufactured laminates. Sci Eng Compos Mater 2015;22(2):115–29. http://dx.doi.org/10.1515/secm-2013-0322.

[16] Chen Q, Ye Y, Qian S, Xu Q, Qu W, Song X, Ke Y. Modeling on the effect of automated fiber placement induced gaps in curved composite laminates. Compos Struct 2024;328(October 2023):117721. http://dx.doi.org/10.1016/j.compstruct.2023.117721.

[17] Groh RM, Wu KC. Nonlinear buckling and postbuckling analysis of tow-steered composite cylinders with cutouts. AIAA J 2022;60(9):5533–46.

[18] Jamora V, Wu K, Kravchenko O. Residual deformation analysis in composite shell structures manufactured using automated fiber placement. Compos Struct 2020;248:112482. http://dx.doi.org/10.1016/j.compstruct.2020.112482, URL https://www.sciencedirect.com/science/article/pii/S0263822319343521.

[19] Pantoji S, Kassapoglou C, Peeters D. Predicting gaps and overlaps in automated fiber placement composites by measuring sources of manufacturing process variations. Compos Part B: Eng 2025;291:111891. http://dx.doi.org/10.1016/j.compositesb.2024.111891, URL https://www.sciencedirect.com/science/article/pii/S1359836824007030.

[20] Jamora VC, Sherin CM, Dong S, Bhattacharjee B, Kaipa K, Kravchenko OG. The effect of prepreg laminate thickness on transverse fiber tow deformation during the deposition of AFP composites. Compos Part A: Appl Sci Manuf 2026;201:109443. http://dx.doi.org/10.1016/j.compositesa.2025.109443, URL https://www.sciencedirect.com/science/article/pii/S1359835X25007389.

[21] Pantoji S, Kassapoglou C, Peeters D. Measuring sources of manufacturing process variations in automated fiber placement composites. International Committee on Composite Materials; 2023, URL https://www.scopus.com/inward/record.uri?eid=2-s2.0-85187541692&partnerID=40&md5=29b7e8002897dc39e35545ee6209f479.

[22] Pantoji S, Peeters D, Kassapoglou C. Experimental dataset about manufacturing process variations in automated fiber placement composites. 2024, http://dx.doi.org/10.4121/ee651378-82a8-4cf3-bbbb-3237dd1e380d.v2.

[23] Metropolis N, Rosenbluth AW, Rosenbluth MN, Teller AH, Teller E. Equation of state calculations by fast computing machines. J Chem Phys 1953;21(6):1087–92.